Ability of Detecting Small Fishing Boats by ALOS-PALSAR Based on CFAR and Multi-Look Cross-Correlation Techniques

Kazuo Ouchi [(1)], **Seong In Hwang** [(1)], **Haipeng Wang** [(2)], **Munetoshi Iwakiri** [(1)]

[(1)] Department of Computer Science, School of Electrical and Computer Engineering, National Defense Academy 1-10-20 Hashirimizu, Yokosuka, Kanagawa 239-8686, Japan, E-mail: ouchi@nda.ac.jp

[(2)] Key Laboratory of Wave Scattering and Remote Sensing, Department of Communication Science and Engineering Fudan University, Shanghai 200433, China, E-mail: hpwang@fudan.edu.cn

Abstract

The purpose of this study is to examine the ability of the PALSAR (Phased Array L-band Synthetic Aperture Radar) on board of the ALOS (Advanced Land Observing Satellite) to detect fishing boats whose sizes are comparable with the SAR resolution scale. The algorithms used for this ship detection experiment are CFAR (Constant False Alarm Rate) with the Weibull distribution for the noise model, MLCC (Multi-Look Cross-Correlation) and CCF (Cross-Correlation Function) of HH- and HV-polarization images. The results indicate that the most suitable mode was the FBS (Fine Beam Single) 34.3, followed by the FBS 21.5, where the numbers after FBS are the nominal off-nadir angles. It is difficult to confirm the images of the boats in the co-polarization images of FBD 41.5 and PLR 20.5, but possible images were observed in cross-polarization images. The CCF (Cross-Correlation Function) of the HH- and HV-polarization images improved the detectability.

keywords : Ship detection, SAR, CFAR, MLCC (Multi-Look Cross-Correlation), Polarimetric Data

1. INTRODUCTION

In recent years, there have been some advance in developing ship detection algorithms by incorporating AIS (Automatic Identification System), ground-based maritime radars and SARs for ocean traffic monitoring, fishing control and identification of ships responsible for oil pollution [1]. Most of ships used for these previous experiments were large compared with the SAR resolution cell, and little work was reported on the detection of ships of sizes comparable with the resolution cell. Thus, it is a challenging work to investigate the ability of spaceborne SARs to detect small boats.

During the Cal/Val stage of ALOS-PALSAR in 2006, we deployed three small fishing boats in the Tosa Bay in Kochi, Japan, for the purpose of testing the ability of PALSAR to extract small boats by means of CFAR, MLCC and CCF techniques. The size of the boats deployed for the experiment were of the order of the SAR resolution cell (approximately 4-8 m in azimuth and 19 m in slant-range). During the time of PALSAR observation over the test site, three fishing boats separated by 50 m in the azimuth direction were cruising with a speed of 8 knots in the range direction. The same experiment was repeated 4 times for the different modes, including FBD 41.5, FBS 21.5, FBS3 4.3 and PLR 20.5. The CFAR algorithm with Weibull distribution for the noise model was applied to full-look images and MLCC to the 2-look images of each mode. Furher, the CCF (Cross-Correlation Function) between HH- and HV-polarization PLR images was examined. Detectability assessment was made by SNR (Signal to background Noise Ratio) values, and comparison was made in terms of different PALSAR modes and different ship detection algorithms.

2. DESCRIPTION OF EXPERIMENTS

2.1. Fishing Boats

Three types of fishing boats were deployed for the experiment. The largest type was Type Ia and Ib, followed by Type IIa and IIb, and the smallest type was Type IIIa and IIIb. The sizes and tonnage of the boats are listed in Tab.1. The hulls of all boats were made of FRP (Fiber Reinforced Plastics) with attached winches and fishing equipments on deck. Fig.1 is an example of the boats of Type I. Other types of boats were similar in shape but in different sizes.

2.2. Meteorological Data

Tab.2 shows the observation dates, deployed fishing boats, and the wave and wind data at the times of SAR data acquisition. The observation times varied depending on the dates but centered at 13:30 $\pm$10 min. (Universal Time), corresponding to 10:30 pm at local time. The wave data were suppled by NOWPHAS (Nationwide Ocean Wave information for Ports and HArbourS) at the Kochi Harbour located at approximately 13 km west of the observation area. The wave data at the sea closer to the experimental area were not available, but *in-situ* visual observation at the

Table 1
Specification of three types of fishing boats used for the PALSAR ship detection experiment.

Sizes	Type I	Type II	Type III
Length (m)	a 12.0 b 14.6	a 10.7 b 11.9	a 8.0 b 9.2
Width (m)	a 3.0 b 4.0	a 3.2 b 3.2	a 2.4 b 2.5
Depth (m)	a 1.2 b 2.0	a 1.1 b 1.0	a 0.8 b 1.1
Tonnage (tons)	a 11.2 b 12.0	a 6.6 b 9.7	a 2.2 b 3.2

Figure 1. A picture of a fishing boat of Type Ia deployed in the experiment.

times of PALSAR data acquisition agreed roughly with the data in Tab.2, *i.e.*, the sea were calm without much wind except the PLR 20.5 data acquisition time. The wind data were measured at a station close to the experimental site, and were supplied by the JWA (Japan Weather Agency).

2.3. Cruising Data

On each observation date, three fishing boats of Type I, II and III were cruising at an angle approximately 8° from the range direction away from the radar. The cruising speed was 8 knots (4.12 m/s). The starting position of Type I was at a distance approximately 1 km from the shore, followed by Type II and Type III boats, each of which were separated by 50 m. At about 10 minutes before the expected time of PALSAR data acquisition, Type I boat started cruising toward the designated port, and at a beach close to the port, a triangular trihedral corner reflector of size 2 m was placed for the Cal/Val purpose. From the cruising speed and the starting time interval, the images of the boats should, in principle, be separated by 494 m in the range direction. However, there were some uncertainties on the exact starting times and positions which, to some extent, depended on the captains of the boats. The images should also be shifted in the azimuth direction due to the slant-range velocity component. This shift is in the range of 165 m and 370 m for incidence angles of 22° and 42° respectively.

2.4. PALSAR Data

The four sets of raw data at the times of PALSAR data acquisition were processed to produce SLC (Slant-Range-Complex) images by the PulSAR SAR processor [2]. For the amplitude and CFAR based ship detection, full-look images were produced with azimuth resolution of 4.5 m (5.0 m for PLR), and 2-look images of resolution 9.0 m were produced with non-overlapping sub-apertures for the MLCC based ship detection. Slant-range resolution was 5.0 m for FBS and FBD, and 10.0 m for PLR.

Table 2
Observation dates, deployed boats, and meteorological data at the times of SAR data acquisition ($\pm$ 30 min.). $H_{1/3}$(m) is the significant waveheight, T_W(s) is the significant wave period, Φ_W ($^\circ$) is the wave direction from north, and WDS is the wind direction followed by the wind speed (m/s).

Dates	19 June	21 June	30 July	06 Aug.
Modes	FBD 41.5	FBS 21.5	FBS 34.3	PLR 20.5
Boat Types	Ia, IIa IIIb	Ia, IIa IIIa	Ib, IIa IIIa	Ib, IIb IIIb
$H_{1/3}$	N/A	0.52	0.36	0.83
T_W	N/A	5.8	7.6	8.5
Φ_W	N/A	154	145	137
WDS	NW 2	NNW 2	N 1	N 2

2.5. CFAR, MLCC and CCF

CFAR is essentially a noise reduction filter in which an expected PDF (Probability Density Function) is subtracted from the observed PDF to extract targets by thresholding [3]. Images to be enhanced may be embedded in noise, but should have amplitude larger than the noise. Adaptive *K*-distribution or Weibull distribution is used for the noise PDF since they fit observed sea clutter well. In the present experiment, the Weibull distribution was used for the noise model.

MLCC is a technique of image extraction, where multi-look SAR images are cross-correlated using a moving window [4]. Images of ships, for example, generally possess high degree of inter-look correlation, while the inter-look images of surrounding sea surface are not correlated. An advantage of this method is that the images of amplitude comparable with speckle noise can be extracted as long as they are correlated. The disadvantage is a loss of spatial resolution by multi-looking. If ocean waves are present, the inter-look wave images also yield high correlation, and ships may not easily be recognized.

CCF can be a useful technique in ship detection if polarimetric data are available. In this experiment, we examined the SNR of a coherence image (degree of correlation) between HH- and HV-polarization amplitude images.

3. RESULTS AND DISCUSSIONS

The SNR values for the images of fishing boats are shown in Tab.3, where "N/V" implies that images of boats are not

Table 3
SNR (Signal to background Noise Ratio) of the images of fishing boats in the original amplitude images, coherence images after MLCC, and the images after CFAR, where "N/V" stands for "Not Visible", and "CCF (HH-HV)" in PLR 20.5 data means the Cross-Correlaton Function between HH- and HV-polarization images.

FBD (HH) 41.5	Type Ia	Type IIa	Type IIIb
Amplitude	N/V	N/V	N/V
MLCC	N/V	N/V	N/V
CFAR	N/V	N/V	N/V
FBD (HV) 41.5	Type Ia	Type IIa	Type IIIb
Amplitude	7.3	N/V	N/V
MLCC	21.3	N/V	N/V
CFAR	23.2	N/V	N/V
FBS (HH) 21.5	Type Ia	Type IIa	Type IIIa
Amplitude	N/V	6.2	10.2
MLCC	9.3	9.4	16.4
CFAR	N/V	13.4	23.8
FBS (HH) 34.3	Type Ib	Type IIa	Type IIIa
Amplitude	12.1	7.8	9.9
MLCC	16.8	11.4	13.8
CFAR	29.5	23.9	25.8
PLR 20.5	Type Ib	Type IIb	Type IIIb
Amplitude (HH/VV)	N/V	N/V	N/V
Amplitude (HV)	10.0	N/V	N/V
MLCC (HH/VV/HV)	N/V	N/V	N/V
CFAR	18.3	N/V	N/V
CCF (HH-HV)	20.8	N/V	N/V

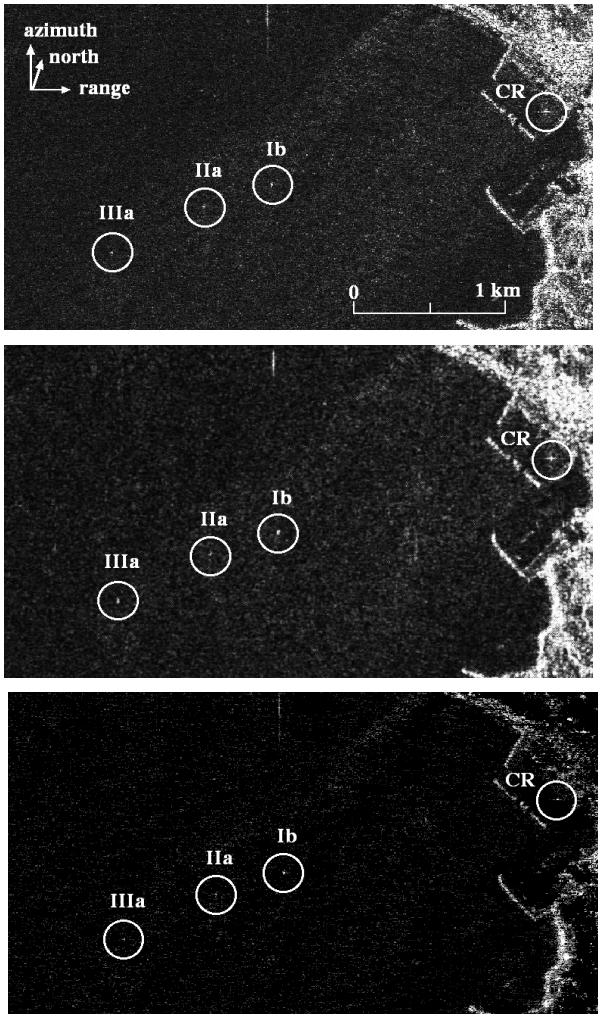

Figure 2. From top to bottom: FBS (HH) 34.3 amplitude image, coherence image after MLCC, and amplitude image after CFAR. The three boats and triangle trihedral corner reflector (CR) are visible.

visible or uncertain, *i.e.*, the image amplitudes are in a noise level. Among all sets of data, the highest detectability in amplitude images was found in the FBS 32.3 (HH) image shown in Fig.2. The SNR values of Type Ib, IIa and IIIa in the amplitude image at the top of Fig.2 are 12.1, 7.8 and 9.9 respectively. No ship wakes were visible in all sets of data. The middle of Fig.2 shows the coherence image after MLCC is applied to the amplitude image. The moving window size was 3×3 by taking into account the size of fishing boats. The SNR values increased to 16.8, 11.4 and 13.8 for the images of Type Ib, IIa and IIa respectively. The SNR, and hence the detectability increased significantly to 29.5, 23.9 and 15.8 in the respective order in the images after CFAR shown in the bottom of Fig.2. Thus, CFAR is proven to be a powerful technique to decrease false alarm rate in ship detection when images of ships are visible. This is the reason why the most of commercial ship detection algorithms are based on CFAR.

The top of Fig.3 is the FBS 21.5 (HH) image, where the boats of Type IIa and IIa are visible, but Type Ia is embedded in noise caused by local wind-roughened ocean surface. CFAR cannot detect the ship of Type Ia as in the bottom of Fig.3 since it reduces noise as well as the boat's image if the image amplitude is in the noise level. However, MLCC, which can extract inter-look correlated images, is able to detect the ship as shown in the middle of Fig.3. This is a good example to illustrate the characteristics of MLCC and CFAR.

The PLR (HH) amplitude image is shown in the top of Fig.4. All boats are embedded in shoaling wave images, and are not visible in both the HH and VV images. The HV image in the middle of Fig.4 shows a boat which is considered to be Type Ia. This is because the radar backscatter from a boat is dominated by multiple scattering which is responsible for strong radar returns at HV-polarization, so that the image of the boat has higher amplitude than that of the surrounding sea surface of which the dominant backscatter is surface scattering. The image of the boat should be present in the HH image, but it is immersed in wave images. It can be extracted and enhanced by cross-

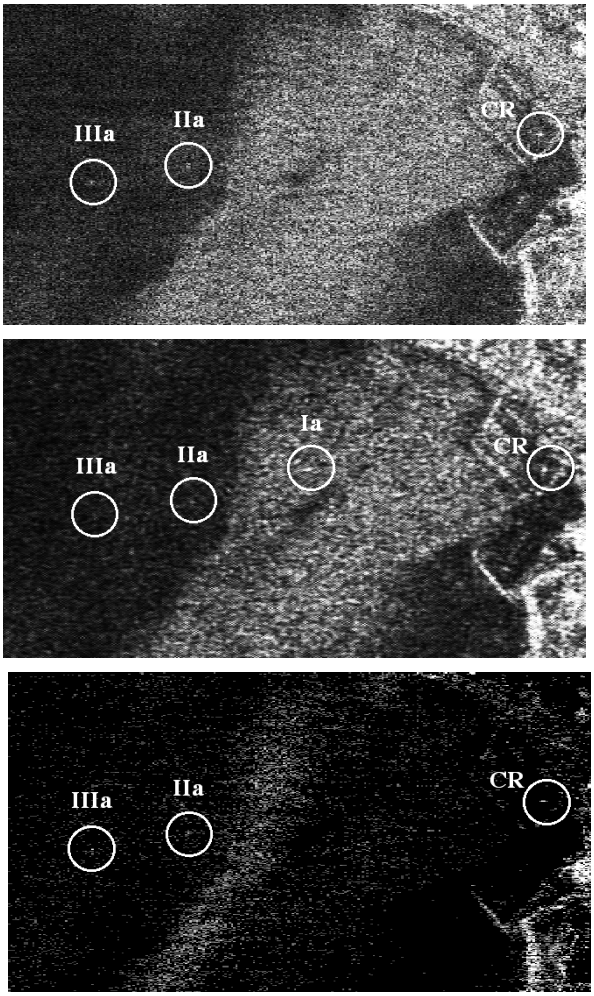

Figure 3. From top to bottom: FBS (HH) 21.5 amplitude image, coherence image after MLCC, and amplitude image after CFAR.

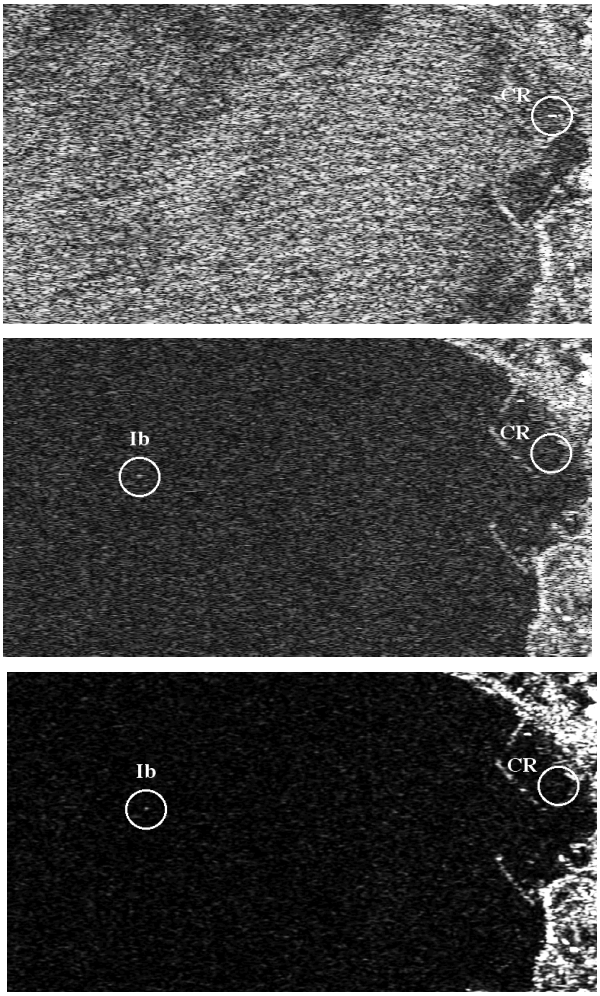

Figure 4. From top to bottom: PLR (HH) 20.5 amplitude image, PLR (HV) amplitude image, and coherence image after cross-correlation of HH and HV images.

correlating the HH image with HV image as shown in the bottom of Fig.4. It should be noted that MLCC could not extract the boats in the PLR data. For ship detection, SARs at incidence angles around $40°$-$60°$ with HH-polarization are regarded as preferable, and the present results appear to show this trend. However, no definite conclusion can be drawn because the sea surface conditions were different at each data acquisition times.

4. CONCLUSIONS

In this paper, the results of initial assessment in detecting small fishing boats from ALOS-PALSAR data are presented. Both the algorithms of MLCC and CFAR performed well in the FBS and FBD modes, highlighting their characteristics, *i.e.*, extraction of boats embedded in noise by MLCC, and high SNR by CFAR. The CCF algorithm using HH- and HV polarization amplitude images was also shown to be effective. We have analyzed only a limited amount of data, but the present results demonstrate the ability of PALSAR in ship detection in which the sizes of ships are comparable with the resolution scale.

REFERENCES

[1] H. Gredanus and N. Kourti, "Findings of the DECLIMS Project - Detection and Classification of Marine Traffic Control," *Proc. SEASAR 2006, Frascati, Italy (ESA SP-613)*, 2006.

[2] A.M. Smith, "A New Approach to Range-Doppler SAR Processing" *Int. J. Remote Sens.*, vol.12, pp.235-251, 1991.

[3] M. Sekine and Y. Mao, *Weibull Radar Clutter*, Peter Peregrinus, London, 1990.

[4] K. Ouchi et al, "Ship Detection Based on Coherence Images Derived from Cross-Correlation of Multilook SAR Images," *IEEE Trans. Geosci. Remote Sens. Lett.*, vol.1, pp.184-187, 2004.